Ultrafast laser machining – process optimization and applications

[a]Norman Hodgson, [b]Albrecht Steinkopff, [a]Sebastian Heming, [a]Hortense Allegre, [b]Hatim Haloui, [a]Tony S. Lee, [a]Michael Laha, [b]Joris van Nunen
[a]Coherent, Inc., 5100 Patrick Henry Drive, Santa Clara, CA 94505, USA;
[b]Coherent Kaiserslautern GmbH, Opelstrasse 10, 67661 Kaiserslautern, Germany

ABSTRACT

Over the last decade industrial ultrafast lasers with pulse durations between 300 fs and 10 ps, average output powers of up to 150 W and single pulse energies in the range of 10 to 250 µJ have been deployed in various industrial applications that require microscopic material removal within small areas with minimum heat affected zones. This paper will provide a detailed understanding of the influence of laser wavelength, pulse duration, pulse fluence and the temporal distribution of the laser pulses (i.e. seeder burst mode operation) on the speed and quality of the machining process. Experimental data for more than 25 materials commonly used in micro-machining applications have led to guidelines for optimizing ultrafast laser machining processes. A review of the industrial ultrafast laser market and a discussion of the main applications are also provided.
Keywords: ultrafast laser processing, ultrafast laser ablation, ultrafast laser machining, heat affected zone, optimum pulse fluence, burst mode, picosecond laser processing, femtosecond laser processing

1. INTRODUCTION

The use of ultrafast lasers for industrial material processing has increased considerably in the last ten years due to the advent of medium-to-high power Nd and Yb-based amplifier systems with output powers of up to 150 W, pulse durations between 300 fs and 15 ps, and repetition rates of up to several MHz[1]. The main advantage of using ultrafast pulses for ablation is the small heat affected zone (HAZ), combined with an increased ablation rate[2-4] for pulses shorter than about 15 ps. Over the last decade, industrial ultrafast diode-pumped solid state and Yb-doped fiber lasers have penetrated the micro-processing market[1,5] reaching an annual revenue of about 380 M$ in 2020. Figure 1 shows the distribution of the 2020 revenue across pulse durations and power levels. Outside of the ophthalmic market segment (LASIK, cataract surgery, and corneal transplant surgery), most of micro-processing applications use picosecond lasers with output powers in the infrared wavelength range of up to 150 W. At present only about 25 % of non-ophthalmic micro-processing applications are served by femtosecond lasers with pulse durations between 300 and 800 fs. Both pulse duration areas have shown a strong CAGR of greater 10 % over the last five years, and it is expected that this growth rate will stay stable through 2025 and potentially increase with the advent of new applications.

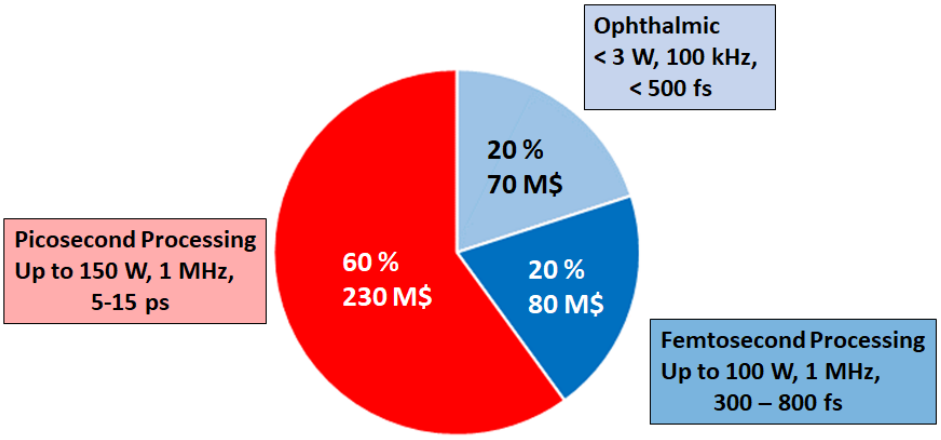

Figure 1. Distribution of 2020 annual revenue in ultrafast lasers for micro-processing[1]. Data in Ref. 1 were modified to adjust for the decrease of the ophthalmic market over the last 5 years.

Laser Applications in Microelectronic and Optoelectronic Manufacturing (LAMOM) XXVI, edited by Carlos Molpeceres, Jie Qiao, Aiko Narazaki, Proc. of SPIE Vol. 11673, 1167308
 · doi: 10.1117/12.2584178

The main driver for using ultrafast micro-processing lasers is the micro-electronic market with flat panel display manufacturing being at the top. Both ps and fs lasers are used here to cut the multilayered display foils as well as for display repairs. Ultrafast lasers are also seeing increased adaption in wafer dicing, de-paneling and via drilling in this market. In the materials processing market segment, the applications are spread over a wide variety of applications where the short pulse durations provide an advantage in processing quality. Examples are stent cutting, glass cutting, marking, including black marking and intra-glass marking, cutting of composite materials. Again, picosecond lasers are mostly used in materials processing, except for stent cutting and texturing, which are femtosecond laser application. Many novel applications have emerged recently that require femtosecond pulses and may play a bigger role in industrial ultrafast processing in the future. Among those are micro-structuring to generate hydrophobic surfaces, glass-to-glass and glass-to-metal welding, and waveguide writing in optical materials.

At present, more than 90 % of the industrial ultrafast laser micro-processing applications are based on laser ablation, which requires careful optimization of the laser pulse fluence to maximize the process speed and minimize the heat affected zone (HAZ). In the following, we will discuss the interaction of the ultrafast laser pulse with the material and how ablation rates and HAZ depend on pulse fluence, laser wavelength, pulse duration, and repetition rate.

2. THEORY OF ULTRAFAST LASER ABLATION

For materials that exhibit free electrons, such as metals and semiconductors, the interaction of the ultrafast pulse with the material can be described by the Two-Temperature Model (TTM), which describes the temporal and spatial change in electron gas and lattice temperatures[6-9]. The incident photons are absorbed by the electrons and subsequent transfer of the energy to the lattice occurs with a time constant referred to as the electron-phonon relaxation time. If we assume an ultrafast laser pulse with absorbed intensity I(t) with a Gaussian spatial profile, the two coupled differential equations for electron gas temperature T_e and lattice temperature T_l read[10]:

$$\frac{\partial T_e}{\partial t} = \frac{1}{C_e}\nabla(K_e \nabla T_e) - \frac{1}{\tau}(T_e - T_l) + \frac{\alpha}{C_e} A\, I(t) e^{-2r^2/w^2}\, e^{-\alpha z} \quad (1)$$

$$\frac{\partial T_l}{\partial t} = \frac{1}{C_l}\nabla(K_l \nabla T_l) + \frac{1}{\tau}\frac{C_e}{C_l}(T_e - T_l) \quad (2)$$

where C_e, C_l and K_e, K_l are the heat capacities and thermal conductivities of electron gas and lattice, respectively, A is the absorption at the surface and α is the absorption coefficient of the material. For copper, with an absorption coefficient[11] of $\alpha = 0.08223\ nm^{-1}$ at a wavelength of 1 µm, the initial penetration depth of the is about 12 nm. The electron-phonon relaxation time τ (e-p relaxation time) depends on the electron gas temperature[12-14] and, for metals, is typically well below 1 ps at room temperature, but can exceed 10 ps for high electron gas temperatures. For laser ablation, the electron gas temperature can be as high as 10^5 K, due to the low heat capacity of the electrons. Calculated e-p relaxation times for various metals at room temperature and at electron gas temperatures of 10,000 K and 50,000 K are shown in Fig. 2.

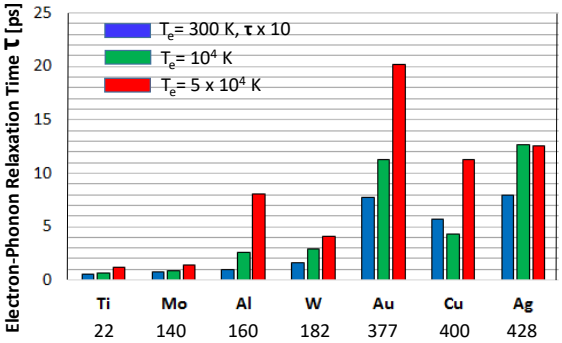

Figure 2. Calculated electron-phonon relaxation times for metals at room temperature (blue bars, multiplied by 10) and at 10,000 K (green bars) and 50,000 K (red bars)[12]. The numbers below the metal symbols are the thermal conductivities at room temperature in W/(m K).

In general, the heat capacity of the electron gas is about 100 times lower compared to the lattice, which according to the second right hand term in Eq. (2) leads to a 100 times slower increase in the lattice temperature as compared to the initial increase in electron temperature. While the light absorption and subsequent thermalization of the electrons occur on a timescale of less than 100 fs, it may take the lattice several tens of picoseconds to reach melting temperature, especially at higher pulse fluences[9]. For this reason, pulse durations shorter than 10 ps will generate very small heat affected zones since during this time energy dissipation via lattice heat conduction can be neglected[15].

The ablated volume per laser pulse can be determined by assuming that ablation only takes place when the fluence is greater than the ablation threshold fluence, with respect to both the beam area and the energy penetration depth[16,17]. For a Gaussian intensity profile with radius w, the beam area where the fluence is above threshold increases logarithmically with pulse fluence (Fig. 3). Slightly above the threshold fluence, ablation is only observed in the central part of the beam, whereas at e^2 times the threshold fluence, the ablated area becomes equal to the Gaussian beam area πw^2. Assuming Beer's exponential law with a penetration depth δ to describe the decrease of the fluence in propagation direction, a similar argument can be made for the depth. Ablation can only occur up to a depth at which the remaining fluence is still above the threshold value. This leads to a similar logarithmic dependence of ablation depth with fluence, with an ablation depth of 2δ when the incident absorbed fluence is e^2 times the threshold fluence[16-19]. This approximation for the ablation depth can be used for fluences that are lower than about 15 times the threshold fluence. For higher pulse fluences, the TTM predicts a linear increase of the ablation depth with the fluence[3,10].

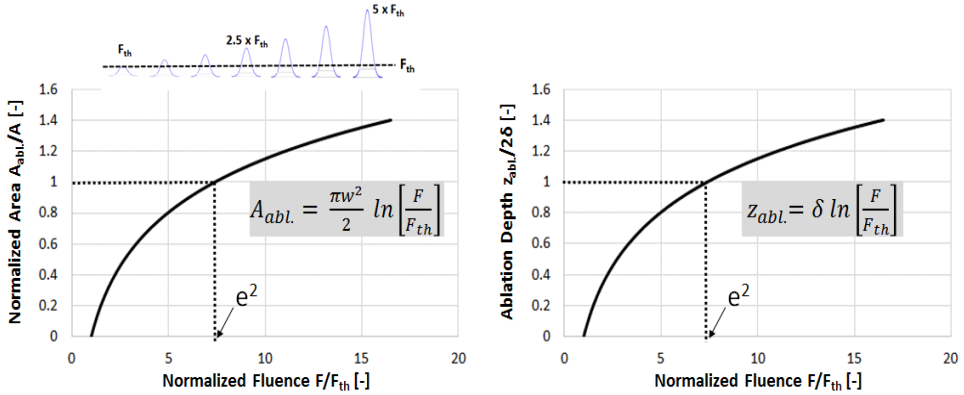

Figure 3. Theoretical dependence of ablated area and ablation depth on the pulse fluence, assuming that ablation takes place in volume areas where the fluence exceeds the threshold fluence. Ablated area (left), where A is the Gaussian beam area, and ablation depth (right).

Although this ablation rate model is based on a very basic assumption, it works very well to predict the measured ablation depths and ablated areas, as will be shown later. The ablated volume per pulse can now be calculated as:

$$V_{abl.} = \frac{\delta\, \pi w^2}{2} \left(ln\left[\frac{F}{F_{th}}\right]\right)^2 \tag{3}$$

We define the ablation rate as the ablated volume per minute and Watt of incident laser power. This parameter describes the efficiency of the laser ablation process. The process speed or throughput is obtained by multiplication with the incident laser power. Dividing Eq. (3) by the average power πw^2 F·f, where f is the pulse repetition rate, and converting the expression to removal per minute, leads to the ablation rate C in mm^3/[W min][17],

$$C = \frac{30\ \delta}{F} \left(ln\left[\frac{F}{F_{th}}\right]\right)^2 \tag{4}$$

where F is the average pulse fluence in J/mm^2, F_{th} is the average threshold fluence in J/mm^2, and δ is the energy penetration depth per pulse in mm. For a Gaussian beam that is focused to a spot diameter 2w, the average pulse fluence is defined as $E/\pi w^2$, where E is the pulse energy. Throughout this paper, we are always using the average pulse fluence.

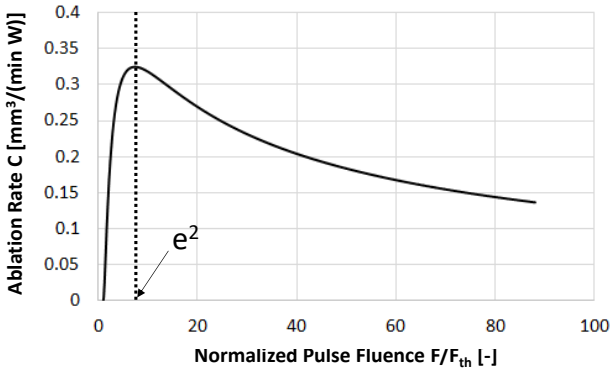

Figure.4. Ablation Rate (ablated volume per minute and per Watt) as a function of the normalized pulse fluence. The ablation rate exhibits a maximum a pulse fluence of e^2 times the threshold fluence.

Typical values for the energy penetration depth per pulse δ are in the range of 10 to 40 nm for metals and semiconductors, and greater 300 nm for dielectrics. Due to the saturation of the ablated volume per pulse with increasing pulse fluence, more volume can be ablated at constant laser power, if the pulse fluence is lowered by increasing the pulse repetition rate (Fig. 4). As was shown by Neuenschwander[17], maximum ablation rate occurs at an optimum pulse fluence $F_{opt} = e^2 F_{th}$. At the optimum fluence, the ablation depth per pulse and the ablated area are given by 2δ and πw^2, respectively, and the maximum ablation rate C_{max} is connected to the optimum fluence via:

$$C_{max} = \frac{120\ \delta}{F_{opt}} \tag{5}$$

This expression allows the determination of the energy penetration depth δ or ablation depth 2δ per pulse at the optimum pulse fluence by measuring the maximum ablation rate only. A comparison to the direct measurement of the ablation depth per pulse can be used to verify the validity of the ablation rate model.

3. MEASURED ABLATION RATES AND THRESHOLD FLUENCES

A modelocked Yb-Fiber MOPA at 1035 nm with an output power of up to 40 W, repetition rates of up to 1 MHz, and maximum pulse energy of 40 µJ was used to generate ablation on 25 different materials[20]. The laser delivered stretched pulses at the exit with 600 ps pulse duration and a spectral bandwidth of 8 nm. The pulses were compressed using a double-pass, dual-grating compressor with variable length to access pulse durations between 400 fs and 18 ps. External frequency doubling in a 3 mm long LBO crystal yielded maximum output powers of 20 W at 517 nm, and maximum pulse fluences of 7 J/cm^2 at the sample surface with spot diameters of 12 µm and 20 µm and pulse durations between 400 fs and 14 ps. For UV generation, the infrared pulses with 350 fs duration were used for frequency-doubling and frequency tripling in two LBO crystals, and the resulting 500 fs long UV pulses were stretched using a double-pass dual-grating compressor with 2,487 lines/mm and a maximum grating separation of 1.14. To accurately determine the ablation rates, rectangular cavities with lengths between 1.5 mm and 3 mm, and widths of 0.3-0.5 mm were ablated using a spot overlap of 60 % in both directions. The cavities were ablated to a maximum depth of about 100 µm, which required around 400 repetitions of the two-dimensional scan pattern. Due to the pulse overlap, each location on the rectangular ablation area is exposed to about 1,600 pulses during the ablation process. The ablation rate was calculated after measuring the ablation depth with a microscope, using only the central square section of the ablated cavity, as shown in Figure 5.

The spot overlap of 60 % was chosen after measuring the ablation rates for 9 different spot overlaps between 10 % and 90 % as a function of fluence and pulse duration and for different materials (Fig. 6). As can be seen, the maximum ablation rates become similar for spot overlaps of 60 % or higher.

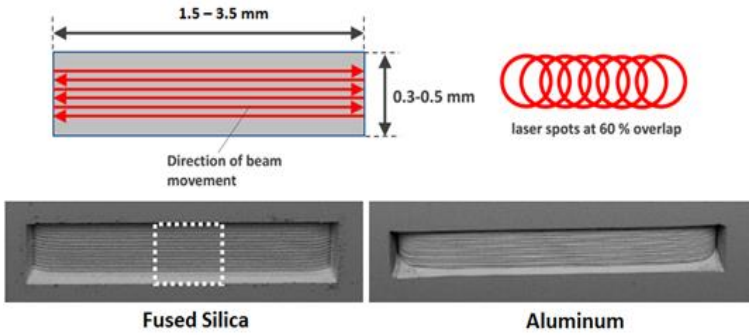

Figure 5. Scan geometry used for ablation with 60 % spot overlap in both directions. The photos show electron microscope images of two cavities in Fused Silica (1.5 mm long) and Aluminum (Al) (3.5 mm long).

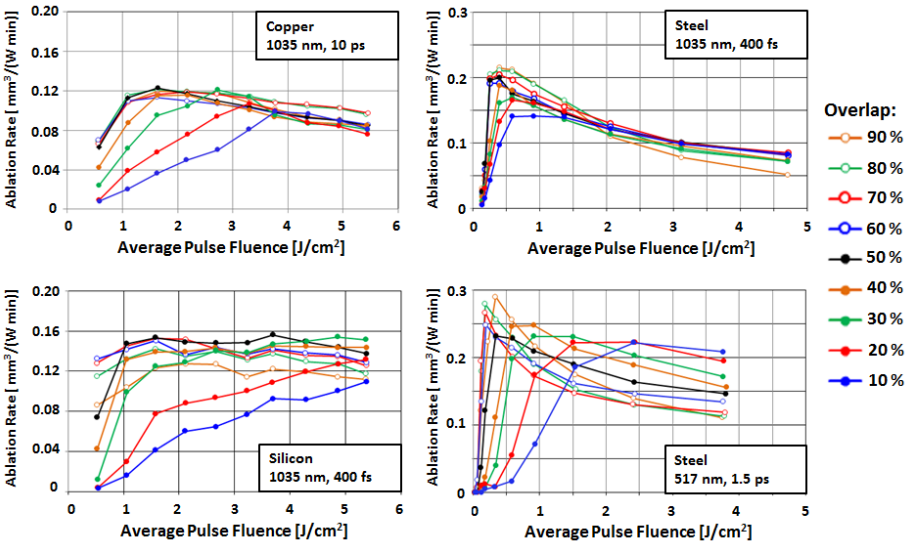

Figure 6. Measured ablation rates as a function of the average pulse fluence for various materials, wavelengths, and pulse durations. The curve parameter is the spot overlap. Spot diameters: 25 µm for Cu, Si at 1035 nm, 18 µm for Steel, and 12 µm for Steel at 517 nm. Repetition rate: 250 kHz.

Note that the maximum of the ablation curves in Fig.7 shift to lower pulse fluences when the pulse overlap is increased. This is due to the increase in the total number of pulses that each location on the surface is exposed to, which results in a decrease of the threshold fluence due to incubation. As a result, the optimum fluence will exhibit a similar decrease. It is well known that the effect of incubation on the threshold fluence can be described by an empirical relationship with the number of pulses per spot[21]. For N pulses per spot, the threshold fluences decreases according to:

$$F_{th}(N) = F_{th}(1)\, N^{S-1} \tag{6}$$

where S is referred to as the incubation parameter. We measured the ablation threshold fluences for various materials for single shot exposure and for 1,600 shots per location. The results for sub-ps pulse durations are shown in Table 1. Some of the corresponding single-shot threshold measurements are depicted in Fig. 7. It is interesting to note that the threshold fluences stay constant below a characteristic pulse duration of about 8 ps. For longer pulses, the heat conduction will increase the affected volume leading to the well-known scaling of the threshold fluence with the square-root of the pulse duration. This behavior agrees with the Two-Temperature-Model which predicts constant damage threshold fluences below a characteristic pulse duration[7,8]. We also measured characteristic pulse durations of about 8 ps for dielectrics such as Fused Silica, BK7 glass, Sapphire, and Kapton polyimide.

Table 1. Measured average ablation threshold fluences F_{th} ($=E_{th}/\pi w^2$) for various materials at 1035 nm, 517 nm and 345 nm, for single shot exposure and for N=1,600 shots per spot, and pulse durations of 400 fs (at 1035 nm and 517 nm) and 500 fs (at 345 nm). The incubation parameter S for 1035 nm was calculated using Eq. 6.

Material Wavelength	$F_{th}(N)$ [J/cm^2] 1035 nm	$F_{th}(1)$ [J/cm^2] 1035 nm	Incubation Factor S 1035 nm	$F_{th}(N)$ [J/cm^2] 517 nm	$F_{th}(N)$ [J/cm^2] 345 nm
Aluminum	0.05	0.14	0.86	0.04	0.025
Copper	0.35	2.0	0.76	0.05	0.05
Gold	0.25	1.4	0.77	0.08	0.08
Molybdenum	0.15	0.2	0.96	0.08	0.08
Steel	0.10	0.15	0.95	0.06	0.03
Nickel	0.09	0.3	0.84	----	0.025
Silicon	0.35	0.38	0.99	1.9	1.5
Fused Silica	2.4	8.0	0.84	0.04	0.025
Sapphire	1.7	15.0	0.70	1.45	1.50

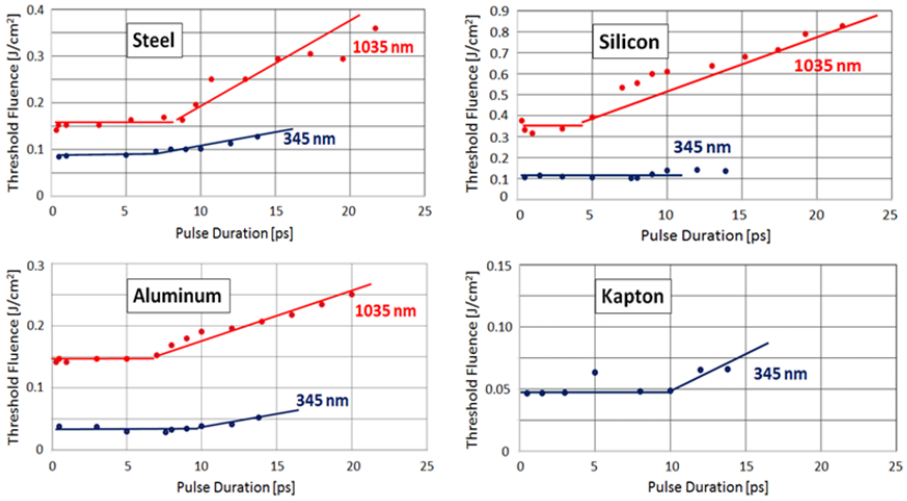

Figure. 7. Measured single-shot damage threshold fluence (average fluence) as a function of pulse duration at 1035 nm and at 345 nm. The lines are shown for guidance. The spot diameter was 36 µm at 1035 nm, and 20 µm at 345 nm.

The relatively large value of the characteristic pulse duration implies that ultrafast laser ablation should exhibit similar HAZ and surface quality for any pulse durations that are shorter than about 10 ps. This is in fact the case as will be shown later. In general, the characteristic pulse duration does not depend on the laser wavelength, since the threshold fluence is solely determined by the interaction of the electrons with the lattice and not by the absorption process between photons and electrons.

We have also measured the ablation depth per pulse at the optimum fluences (which at the optimum fluence is equal to 2δ) by measuring the depth of the ablated cavities and dividing by the number of pulses that were used per location. The measured ablation depths per pulse are in good agreement with the values provided by Eq. 5 using the measured maximum ablation rates and optimum fluences. Compared to the typical spot diameters of tens of microns, the energy penetration depths are very small. Any increase in electron diffusion will therefore increase the depth of the ablated volume and not the diameter. As will be shown later, ablation rates in materials with free electrons can increase by up to a factor 2 when reducing the pulse duration from 10 ps to 300 fs, due to an increase in penetration depth[17-19].

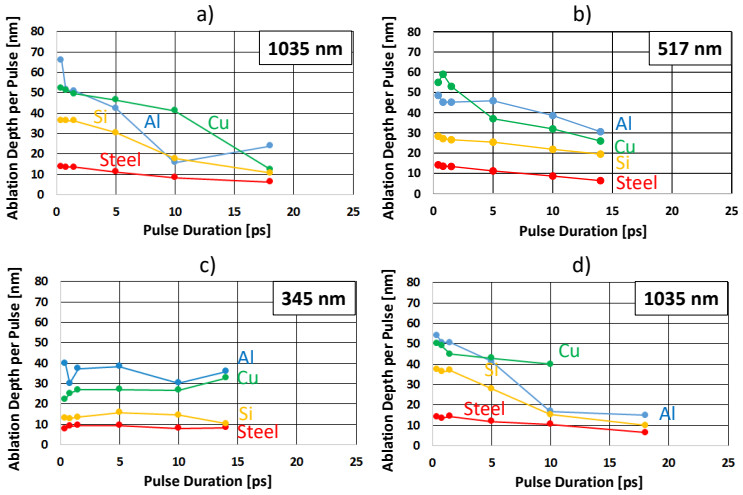

Figure 8. Measured ablation depth per pulse at the optimum pulse fluence at 1035 nm, 517 nm and 345 nm for four materials as a function of the pulse duration. The data in graphs a) - c) were obtained by measuring the depth of the ablated cavity and dividing by the total number of pulses per location. The ablation depths at 1035 nm in graph d) were calculated from the measured ablation rates and optimum fluences by using Eq. 5, with an ablation depth of 2δ. The spot diameter was 36 µm at 1035 nm, and 20 µm at 345 nm.

The measured ablation rates for various materials exhibiting electrons in the conduction band are shown in Figs. 9-11. In general, the measured ablation rates curves show the expected shape predicted by the ablation model discussed above, with an optimum fluence at about 7.4 times the threshold fluence. It is important to note that the ablation rates for metals for sub-ps pulses are only a factor 3 lower as compared to ablation using 100 ns pulses[6]. For wavelengths of 1035 nm and 517 nm, the energy penetration depth δ increases as the pulse duration is decreased with a typical increase by a factor 1.5 - 2 between 10 ps and 400 fs, leading to highest ablation rates for sub-ps pulses. At 345 nm, penetration depths were mostly independent of pulse duration.

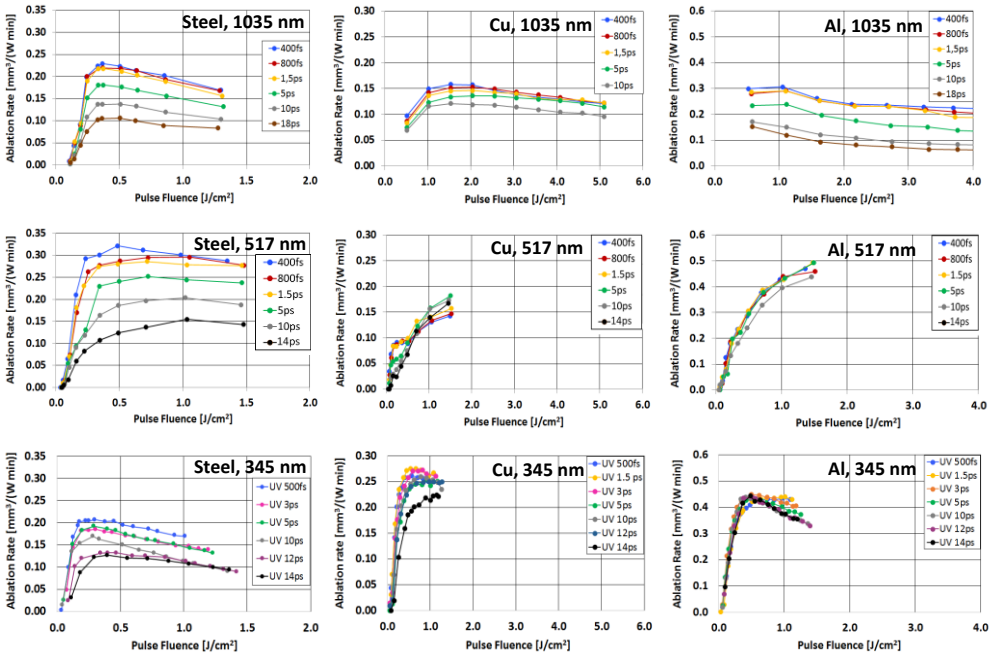

Figure 9. Measured ablation rates as a function of the pulse fluence[20] for Steel (left), Copper (middle), and Aluminum (right) at 1035 nm, 517 nm and 345 nm. The curve parameter is the pulse duration. Spot Diameters: 25 µm at 1035 nm, 12 µm at 517 nm, and 20 µm at 345 nm. Repetition rate: 250 kHz at 1035 nm and 517 nm, and 500 kHz at 345 nm.

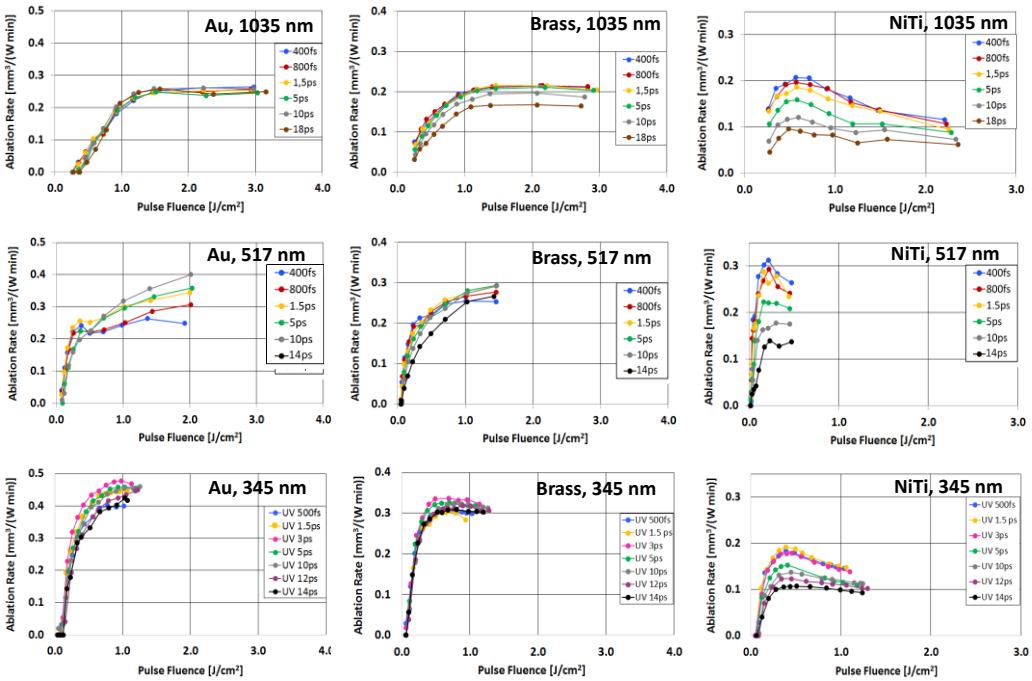

Figure 10. Measured ablation rates as a function of the pulse fluence[20] for Gold (left), Brass (middle), and Nitinol (right) at 1035 nm, 517 nm and 345 nm. The curve parameter is the pulse duration. Spot Diameters: 25 µm at 1035 nm, 12 µm at 517 nm, and 20 µm at 345 nm. Repetition rate: 250 kHz at 1035 nm and 517 nm, and 500 kHz at 345 nm.

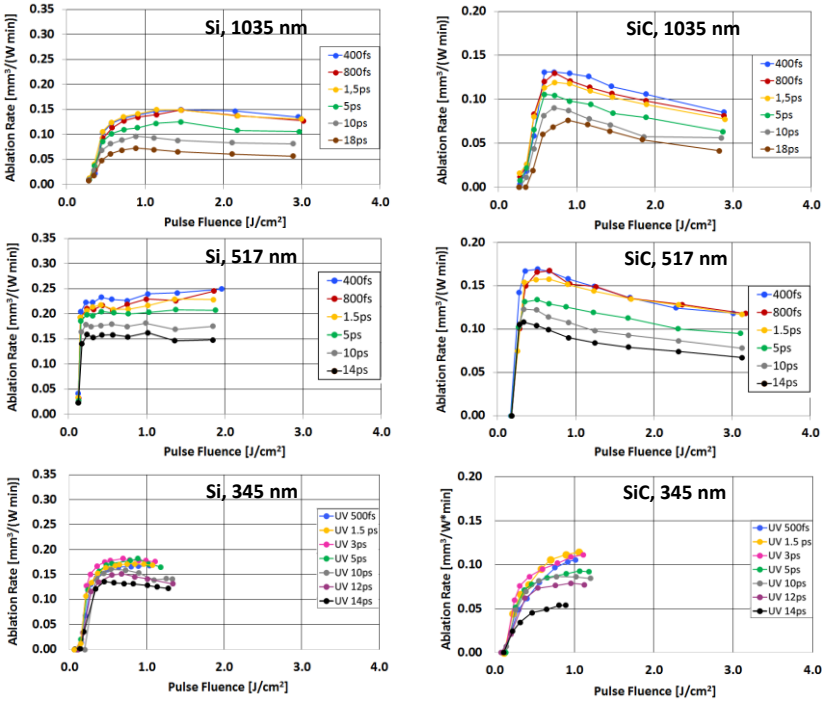

Figure 11. Measured ablation rates as a function of the pulse fluence[20] for Silicon (left), and Silicon Carbide (right) at 1035 nm, 517 nm and 345 nm. The curve parameter is the pulse duration. Spot Diameters: 25 µm at 1035 nm, 12 µm at 517 nm, and 20 µm at 345 nm. Repetition rate: 250 kHz at 1035 nm and 517 nm, and 500 kHz at 345 nm.

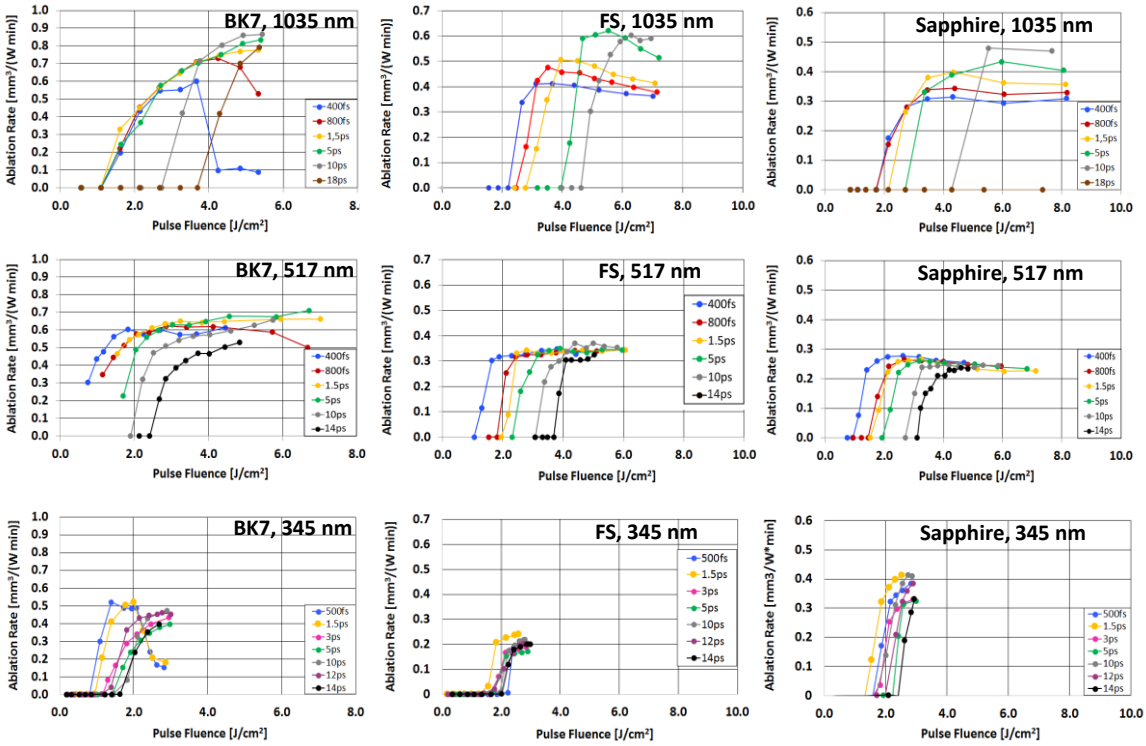

Figure 12. Measured ablation rates as a function of the pulse fluence[20] for BK7 glass, Fused Silica (FS), and Sapphire at 1035 nm, 517 nm and 345 nm. The curve parameter is the pulse duration. Spot Diameters: 25 µm at 1035 nm, 12 µm at 517 nm, and 20 µm at 345 nm. Repetition rate: 250 kHz at 1035 nm and 517 nm, and 500 kHz at 345 nm.

While metals and semiconductor materials exhibit highest ablation rates for sub-ps pulses, the material interaction of the ultrafast pulses ablation behavior is very different for dielectrics that are transparent to the laser wavelength. The lack of free electrons leads to high threshold fluences of several J/cm^2 in the infrared, since free electrons must be generated via photo-ionization, as can be seen in Fig. 12 for BK7, Fused Silica and Sapphire. Sub-picosecond pulses, however, will lead to an optical breakdown at the surface as the pulse fluences are increased. Therefore, the highest ablation rates are attained for pulse duration of several tens of picoseconds. At the green laser wavelength and even more so at the ultraviolet wavelength, the materials become optically absorbing and the preference for longer picosecond pulses disappears. Note that the ablation rate curves at 345 nm in Fig. 12 are limited to fluences below 2.9 J/cm^2, as this was the maximum fluence that could be realized with the experimental set-up.

A summary of the measured maximum ablation rates and corresponding maximum process speeds is shown in Fig. 13 for selected materials. To calculate the processing speeds, we assumed output powers of 100 W, 50 W and 30 W, at 1035 nm, 517 nm and 345 nm, respectively, which represents the state-of-the art of industrial ultrafast lasers. As expected from Eq. 5, the process speeds decrease with decreasing wavelength for most of the materials shown. However, there are exceptions: Nitinol at 517 nm, and plastic materials exhibit much higher process speeds for UV laser ablation due to a strong linear absorption. Examples are Kapton and transparent plastic materials used in flat panel displays, as shown in Fig. 14. Like metals, the plastic materials exhibit very low optimum fluences of about 0.75 J/cm^2 due to the strong linear absorption of ultraviolet light. Considering all materials investigated the general statement can be made that the decision to use a shorter wavelength is not driven by an increase the process speed, but rather, as we will be discussed later, by minimizing HAZ and/or surface roughness.

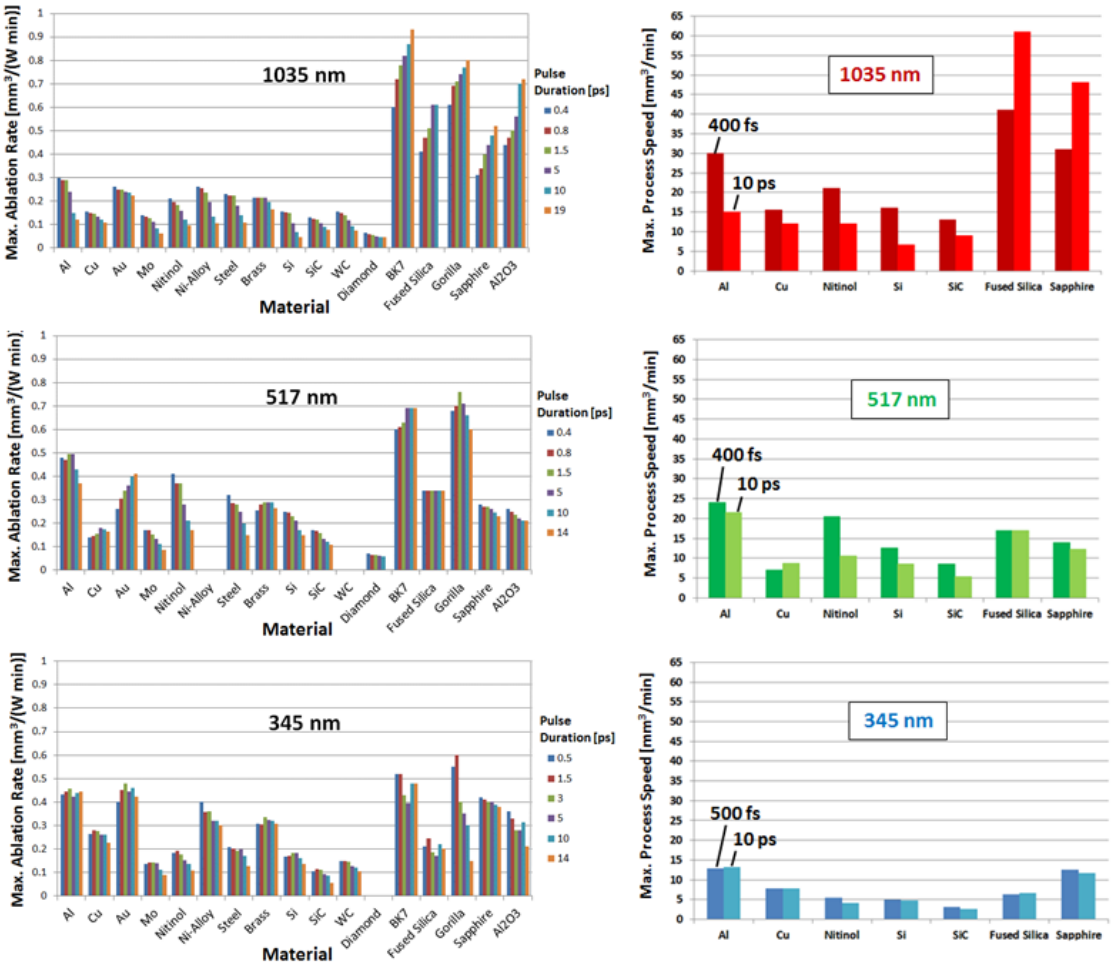

Figure 13. Measured maximum ablation rates in $mm^3/(W\ min)$ (left) and corresponding maximum process speeds in mm^3/min (right) for various materials. The parameter of the bars is the pulse duration, with the shortest pulse duration at the left. To calculate the process speeds, output powers of 100 W, 50 W and 30 W at 1035 nm, 517 nm, and 345 nm were assumed. For Gorilla glass and Al_2O_3 ceramic and pulse durations greater 1.5 ps, the maximum pulse fluences at 345 nm were not high enough to reach the ablation rate maximum. For these two materials, the highest measured rates are shown.

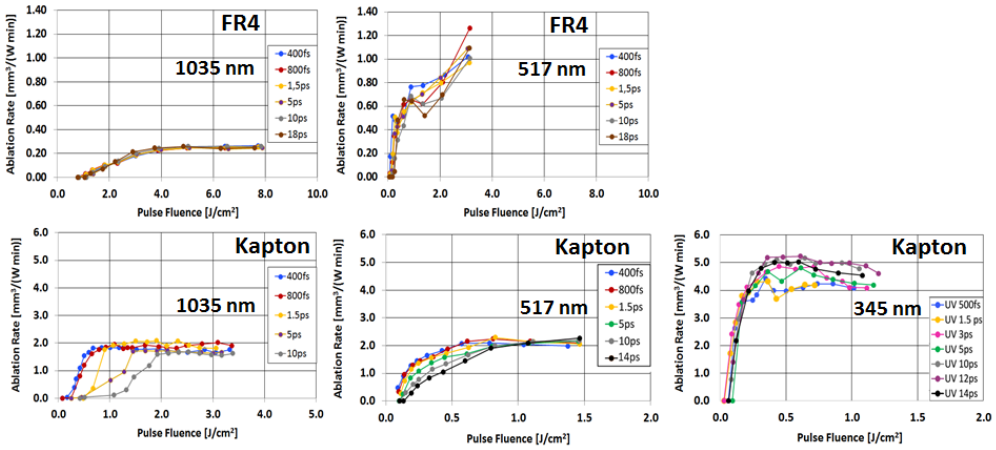

Figure 14. Measured ablation rates as a function of the average pulse fluence for FR4 and Kapton at 1035 nm, 517 nm and 345 nm. The curve parameter is the pulse duration. Spot Diameters: 25 µm at 1035 nm, 12 µm at 517 nm, and 20 µm at 345 nm. Repetition rate: 250 kHz at 1035 nm and 517 nm, and 500 kHz at 345 nm.

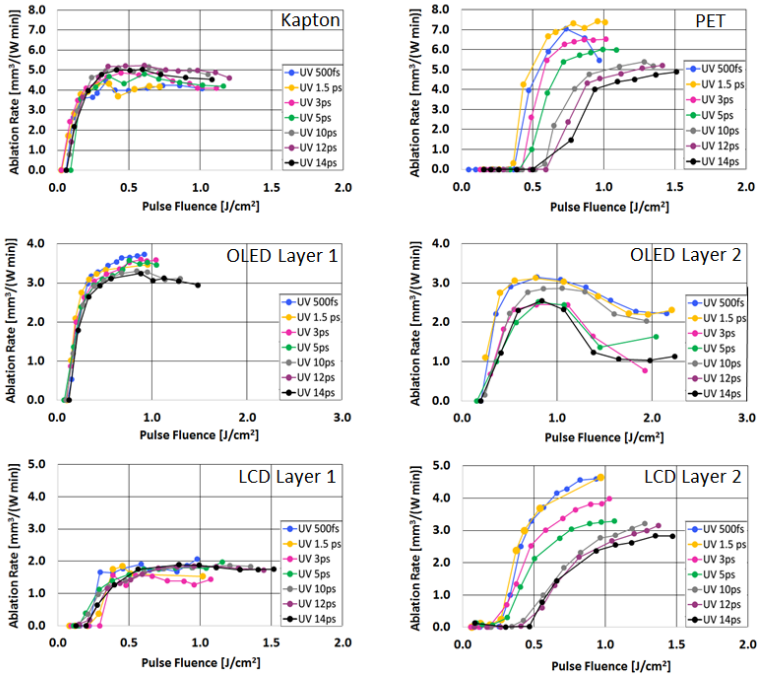

Figure 15. Measured ablation rates as a function of the average pulse fluence for different plastic materials at 345 nm. The curve parameter is the pulse duration. Spot Diameter: 20 µm for all materials, except for OLED Layer 3 (12 µm spot diameter). Repetition rate: 500 kHz.

It is important to note that the optimum pulse fluences for all metals, semiconductors and plastic materials measured were in the range of 0.5 – 1.5 J/cm^2. This poses a challenge for micro-processing since for a typical laser power of 50 – 100 W and a repetition rate of 500 kHz, the average pulse fluences on the material for a 20 µm spot diameter are in the range of 32 to 64 J/cm^2. Reaching the optimum fluence, therefore, requires either much larger spot diameters, or operating at 30-60 times higher repetition rates. If operation at very high multi-MHz repetition rates are not feasible, one possible way to increase the number of pulses per second to tens of millions is to use a burst of amplified seed laser pulses with 10s of ns separation while keeping the temporal distance between bursts at the µs level. We will discuss these optimization schemes in more detail after analyzing the effect of operation near the optimum pulse fluence on the heat affected zone. This scheme allows practical laser triggering in the 100s of kHz domain, while achieving optimum fluence for each individual pulse delivered to the sample at a much higher (multi-MHz) rate.

4. HEAT AFFECTED ZONE AND SURFACE QUALITY

The fact that the damage threshold fluences are constant below pulse duration of about 8 ps leads us to expect that the width of the heat affected zone may also be constant over this range of pulse durations. To investigate this, lines were ablated in several materials as a function of pulse fluence and pulse duration and the HAZ was measured by visual inspection of the ablation edge under a microscope. The lines were ablated using 150 passes, with a pause of 1 second between passes to avoid any melting effects. Figure 16 shows the measured width of the HAZ as a function of the pulse duration for different pulse fluences for Steel and Kapton. In general, for pulses shorter than about 8 ps, the HAZ is independent of the pulse duration when operating at the optimum fluence. As the pulse fluence is increased the HAZ width increases and, in addition, a dependence on the pulse duration will materialize, with shorter pulses providing smaller HAZ at high fluence. However, operating at the optimum fluence of about 7.4 times the ablation threshold fluence will lead to maximum ablation rate and minimizes the HAZ, independent of pulse duration. This is not surprising, since a higher fraction of the energy is transferred into the ablation process instead of being dissipated into the material. The HAZ can be made even smaller for pulse fluences that are below the optimum one, but in this case the ablation rate is also much lower due to a reduction of the width of the ablated line. In addition, there is a linear dependence of the HAZ width on the spot diameter of the laser beam as the example of Kapton in Fig. 16 clearly indicates. Using a small spot diameter is therefore crucial to realize a small HAZ, and the use of a shorter wavelength combines the ability of tighter focusing at

restively large Rayleigh ranges with high quality cuts with minimized thermal damage. This reduction in spot size is especially important for plastics, as these materials are poor conductors leading to larger HAZ. While HAZ widths of around 6-8 µm are standard for metals for a 20 µm spot diameter, the heat affected zone in plastic materials like Kapton or PET can be up to ten times wider. Minimizing the spot diameter by selecting a UV laser wavelength is therefore essential for processing these heat-sensitive materials.

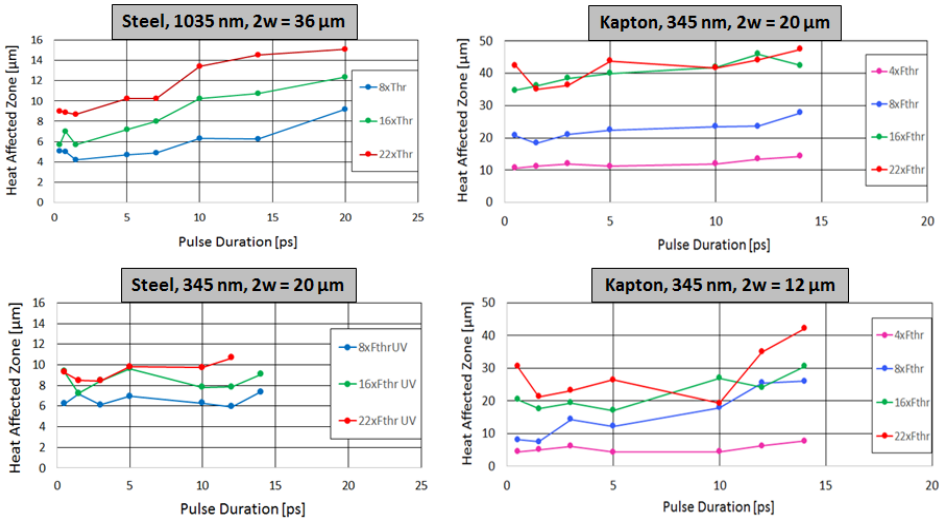

Figure 16. Measured HAZ width of ablated lines as a function of the pulse duration for Steel at different laser wavelengths (left), and for Kapton at 345 nm for different spot diameters (right). Repetition rate of 200 kHz for Steel, and 500 kHz for Kapton. 60 % spot overlap.

The surface quality at the bottom of the ablated cavities was measured with a white light interferometer. The surface roughness (standard deviation) was determined for different materials as a function of pulse duration, wavelength and pulse overlap. Table 2 shows the surface roughness at the optimum pulse fluence for four different materials at 1035 nm and 517 nm, again for a spot overlap of 60 %. Similar to the HAZ, the surface quality is independent of the pulse duration for pulse lengths below about 10 ps. However, the laser wavelength does have an influence and depending on the material the surface roughness may increase or decrease when switching from infrared to a shorter wavelength. Nitinol, for example, exhibits about half the surface roughness when ablated at 517 nm, while ablation of steel at 517 leads to a 2x rougher surface. We also investigated the role of pulse fluence and overlap on the surface roughness. In general, the surface quality improves with increasing fluence and increasing pulse overlap. At very high fluences and pulse overlaps, the reduction of surface roughness is mainly caused by melting. While a small HAZ requires operation at lower pulse fluences, the surface quality is improved when the fluence is increased. However, operation at the optimum fluence can lead to minimum HAZ and low surface roughness, if the correct spot overlap is chosen.

Table 2. Measured surface roughness (standard deviation) in µm for various pulse durations for ablation at the optimum fluence. Four Materials were ablated at wavelengths of 1035 nm and 517 nm.

Material	wavelength [nm]	400 fs	1.5 ps	5 ps	10 ps	14 ps	18 ps
Aluminum	1035	0.70	0.66	0.71	0.67	----	0.60
Aluminum	517	0.65	0.94	1.06	1.09	1.15	----
Steel	1035	1.11	1.13	1.05	1.09	----	1.08
Steel	517	2.00	2.74	2.74	2.01	2.00	----
Nitinol	1035	2.69	2.77	2.44	2.08	-----	1.98
Nitinol	517	1.08	0.97	0.98	0.89	0.82	----
Silicon	1035	2.43	2.48	2.77	3.06	----	2.14
Silicon	517	1.93	1.43	1.44	1.59	1.67	----

5. OPTIMIZATION OF THE ULTRAFAST ABLATION PROCESS

Figure 17 summarizes the measured maximum ablation rates versus the measured optimum pulse fluences for various materials[20] at laser wavelengths of 1035 nm and 345 nm and pulse durations of 10 ps and 400-500 fs. It is apparent that average pulse fluences of around 1 J/cm^2 are required to maximize the ablation efficiency. For a typical laser output power of 100 W in the infrared, and a spot diameter of 25 µm, this means that the laser repetition should be in the 10-20 MHz range. However, the speed of typical galvo mirror scanners is limited to about 10 m/s, which means that at 10 MHz repetition rate, the spot overlap will be 96 % for a 25 µm diameter beam. To reduce the beam overlap to values in the range of 60-80 %, process repetition rates must be reduced to 1-2 MHz, leading to pulse fluences that can be up twenty times higher than the optimum fluence. Operating at these high pulse fluences will lead to a reduction of the process speed by more than a factor of 2 as the process speeds for copper shown in Figure 19 indicate. This graph was generated by using the measured ablation rates at 1035 nm of Fig. 9 and multiplying with four power levels between 30 W and 120 W. For 60 W of laser power at a repetition rate of 500 kHz, the process speed is decreased from about 11 mm^3/min at the optimum fluence of 1.75 J/cm^2 to about 4 mm^3/min at twenty times the optimum fluence.

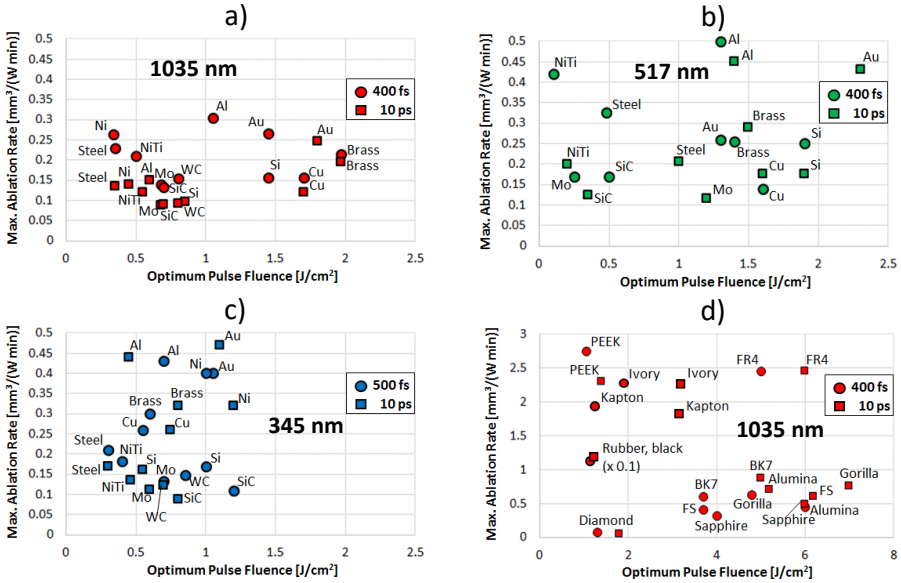

Figure 17. Measured maximum ablation rates versus the optimum pulse fluence at which the maximum ablation rate was measured[20]. Graphs a)-c) are for metals and semiconductors at the three wavelengths. Graph d) shows the measured data for dielectrics at 1035 nm. Large area ablation using 400 ablated layers and 60 % spot overlap.

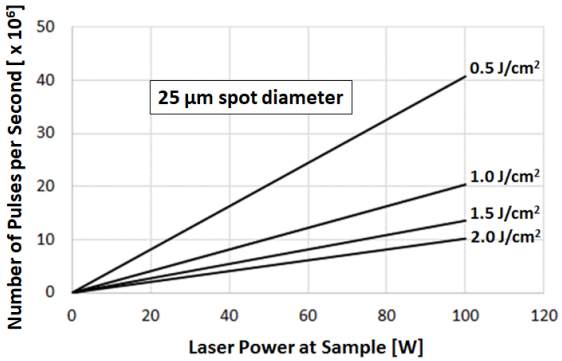

Figure 18. Required number of laser pulses per second as a function of laser power to generate pulse fluences in the range of 0.5 J/cm^2 to 2 J/cm^2 on the sample.

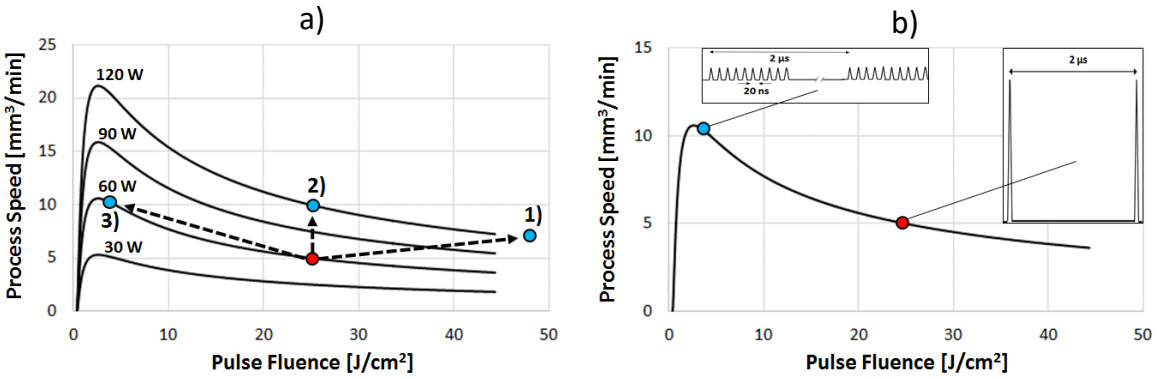

Figure 19. a) Ablation Rates for Copper at 300 fs as a function of pulse fluence for four different average power levels at the sample. Three different routes are shown to increase ablation rate are indicated, starting with 60 W, 500 kHz, and 25 µm spot diameter (red dot): 1) Increasing pump power by a factor 2, 2) Increasing both pump power and repetition rate by a factor of 2, and 3) Increasing repetition rate by a factor of 10 at the same output power, or equivalently, using burst mode operation with 10 pulses per burst. Plot b) shows the change in process speed and the pulse intensity pattern when switching on seeder burst mode with ten pulses and 50 MHz seeder repetition rate.

In general, there are three different ways to increase the process speed of ultrafast micro-processing[22-24], as indicated in Graph a) of Fig.19. For a 60 W laser at 500 kHz using a 25 µm spot diameter, the initial pulse fluence of 24.5 J/cm^2 is about a factor of 10 above the optimum fluence and the process speed is around 5 mm^3/min. The obvious, but least efficient, way to increase the process speed is to double the laser power while maintaining the repetition rate (route 1). In this case the process speed increases by 40 %, but the pulse fluence is doubled leading to much higher HAZ. Doubling both the laser power and the repetition rate, as indicated by route 2), leads to a doubling of the process speed while maintaining the HAZ. The optimum way to increase process speed, however, is represented by route 3) where the repetition rate is increased by a factor 10x to 5 MHz at the same laser power of 60 W. This leads to operation at the optimum fluence to minimize HAZ while increasing process speed by more than a factor of 2.

If operation at high repetition rates is not a workable option due to limited scanner speeds, a workaround is to use seeder burst mode[23] as shown in Figure 19 b). By using bursts of ten seeder pulses with 20 ns separation and staying at a process repetition rate of 500 kHz, the number of pulses per second is the same as for 5 MHz operation, not only resulting in the highest process speed of 11 mm^3/min, but also minimizing the heat affected zone. In general terms, seeder burst mode operation with N pulses per burst will reduce the fluence of individual laser pulses by a factor of N thus moving the operating point towards the optimum fluence to increase the material removal rate and reduce the heat affected zone[22-24].

The basic assumption here is that seeder burst mode operation enables ablation rates that are equal to the ones that would be obtained when operating the laser at a high repetition of 10s of MHz and at the optimum pulse fluence (Fig. 20, route A). This means that we assume that there is no interaction between the intra-burst pulses via the work piece, which from a thermal perspective is true for most metals as the thermal relaxation time within the ablated spot is in the 1-2 ns range. However, the measured ablation rates may be lower due to plasma shielding of individual pulses (Fig.20, route B). For materials with low thermal conductivity, like glasses and polymers, the ablation rate can also be increased due to the thermal interaction between pulses (route C). Which of these three scenarios will be observed depends strongly on the material properties, the number of pulses per burst, the temporal spacing between pulses in the burst, as well as on the geometry of the ablated area. Large ablation areas, for instance, will reduce plasma shielding effects, whereas cutting deep trenches does not allow the plasma plume to escape before the next burst pulse arrives.

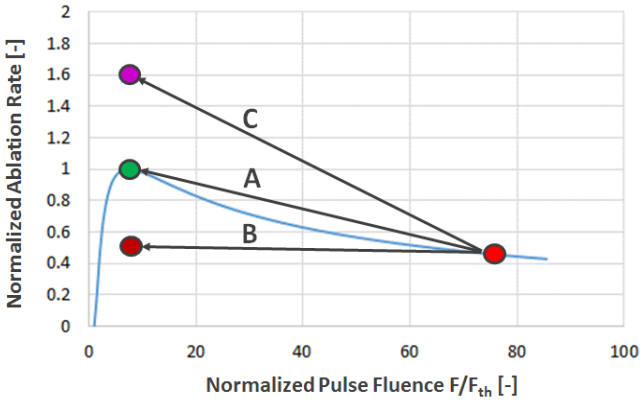

Figure 20. Possible effects on the ablation rate C when switching on burst mode with ten pulses per burst at constant laser power to operate at the optimum pulse fluence. A) no interaction between pulses, B) plasma shielding between pulses, C) interaction between pulses leading to increased ablation depth per pulse.

Figure 21 shows the measured ablation rates for copper and aluminum as a function of the pulse fluence for various number of pulses in the burst. Seeder repetition rate is 60 MHz, generating 16.7 ns temporal separation between pulses in the burst. For both metals, the curves indicate that burst mode operation with 3, 5 and 10 pulses leads to a similar ablation rate as compared to standard single pulse operation. The lower ablation rates for 2 and 4 burst pulses are a result of plasma shielding[25-27]. Time-resolved investigation of the shielding during copper ablation[27] showed that the lower ablation rate is a result of reflection at the plasma plume for even number of seeder burst pulses. As a rule, at least 5 pulses per burst should be used to avoid shielding effects when operating at seeder frequencies around 60 MHz.

For silicon and fused silica, burst mode ablation leads to an increase of the ablation rate over the single-pulse case due to an interaction between the pulses (Fig. 22). For Fused Silica, this can be explained by thermal interaction as the thermal relaxation time of around 10 ns is greater than the pulse separation. For silicon, with very high thermal conductivity, the interaction must be caused by a different, yet unknown, effect. Note that the ablation rate is enhanced by more than a factor of 2 when bursts with 5 or more pulses are used. This means that for the same laser power, and the same number of pulses per second, the ablation depth becomes twice as large in seeder burst mode. An example would be ablation at a repetition rate of 1 MHz in single pulse operation compared to 100 kHz operation using a 10-pulse seeder burst. The later operational mode will result in twice the ablation depth for the same process time and laser power.

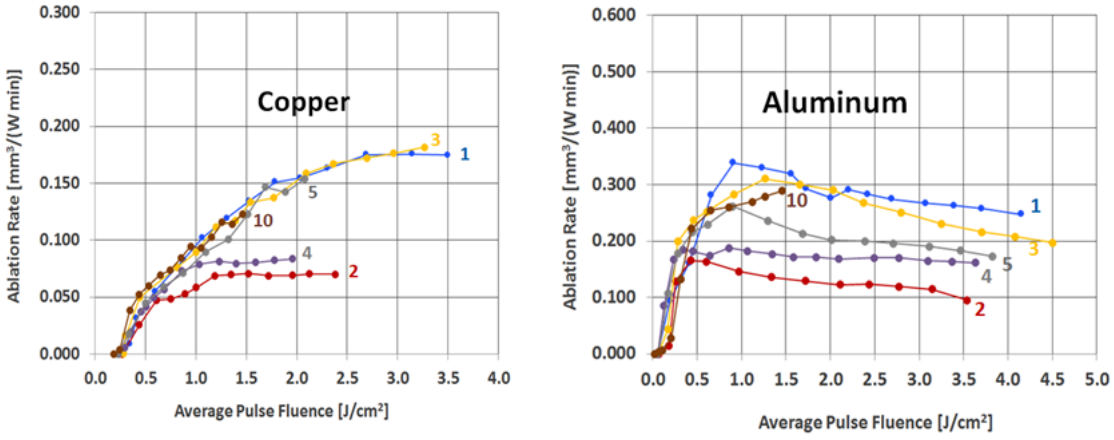

Figure 21. Measured ablation rates at 1035 nm of copper and aluminum as a function of the pulse fluence. Curve parameter is the number of pulses in the burst (at 60 MHz). Process repetition rate was 250 kHz for 1 to 4 pulses, and 200 kHz for 5 and 10 pulses. Spot diameter: 23 µm, 60 % overlap. Large area ablation of 0.5 mm x 1.5 mm with 400 ablation layers[28].

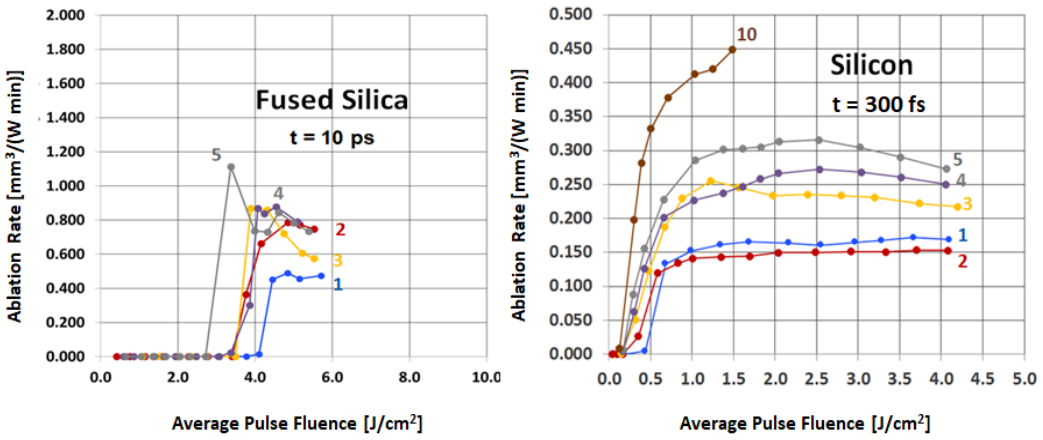

Figure 22. Measured ablation rates of silicon (300 fs pulses) and fused silica (10 ps pulses) as a function of the pulse fluence at 1035 nm. Curve parameter is the number of seeder pulses per burst. Process repetition rate was 250 kHz for 1 to 4 pulses, and 200 kHz for 5 and 10 pulses. Spot diameter: 23 µm, 60 % spot overlap. Large area ablation of 0.5 mm x 1.5 mm with 400 ablation layers[28]

Figure 23 shows measured maximum ablation rates for ten materials in seeder burst mode using a 1035 nm laser with 300 fs pulse duration[28]. Large area ablation (0.5 x 1.5 mm^2) was used with 23 µm spot diameter, 60 % spot overlap and 400 ablation layers. Each bar is the maximum ablation rate for a certain seeder repetition rate and a certain number of pulses per burst. For metals, burst mode operation does generally not increase the maximum ablation rate, meaning that the highest process speed is always attained by using single pulse mode at the optimum pulse fluence. This, however, usually requires a process repetition rate in the 10-20 MHz range. If the process repetition rate must remain in the sub-MHz range, burst mode operation will allow an increase in process speed by reducing the pulse fluence to get closer to the optimum fluence. For semiconductors and dielectrics, burst mode operation will, in addition, lead to an enhancement of the ablation rate compared to single pulse operation. For silicon, this enhancement can be as high as a factor of 5. For metals and dielectrics, seeder burst repetition rates of greater than about 200 MHz do not provide an advantage with respect to the maximally attainable ablation rates. Burst mode operation with GHz seeder repetition rates seems to only result in an increase in ablation efficiency for semiconductor materials and dielectrics with low thermal conductivity[29].

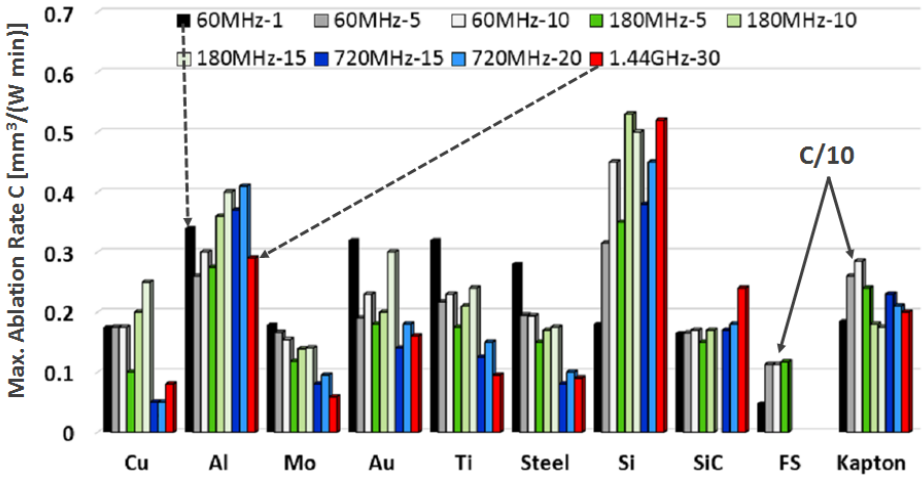

Figure 23. Measured maximum ablation rates for ten materials for various seeder burst repetition rates and number of pulses per burst, as indicated in the legend[28]. 1035 nm laser with 300 fs pulse duration. For Fused silica, 10 ps pulses were used.

6. ULTRAFAST LASER MICRO-PROCESSING APPLICATIONS

Micro-processing applications that require sub-ps pulses are depicted in Figs. 24-26. In ophthalmology, laser output powers of up to 3 W at a wavelength of about 1 µm and pulse durations of around 300 fs are used for corneal flap cutting in LASIK, and lens sack opening and lens fragmentation in cataract surgery. The ophthalmic laser applications represent about 40 % of all applications where industrial femtosecond lasers are used. Pulse energies used for flap cutting are less than 5 µJ, whereas lens fragmentation requires pulse energies of up to 40 µJ. In micro-machining, mature laser processes that require sub-ps pulses are injection nozzle drilling and stent cutting, as shown in Fig. 25. Both applications use infrared lasers with 300 fs pulses and up to 40 W of average power at repetition rates of up to 1 MHz. Two novel applications that require sub-ps pulses and may have considerable growth potential are shown in Fig. 26: Glass welding using femtosecond pulses to generate melt spots at the interface between glasses or between glass and metal, and micro-structuring of metal surfaces by irradiating the surface using a high-power line beam. The micro-structure leads to a hydrophobic surface. Both femtosecond processes require infrared laser pulses with ~ 300 fs duration. Whereas glass welding is a medium power application that requires less than 100 W average power, micro-structuring becomes more efficient at high output powers of up to many hundreds of Watts.

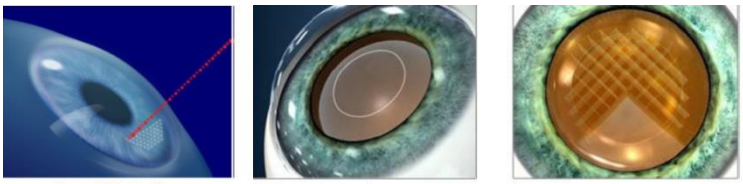

Figure 24. Ophthalmic femtosecond laser processes. Corneal Flap Cutting by generating a plane of bubbles inside the cornea to separate the flap (left). The two right photos depict laser processes used in cataract surgery: capsulotomy to open the lens sack and lens fragmentation to enable removal.

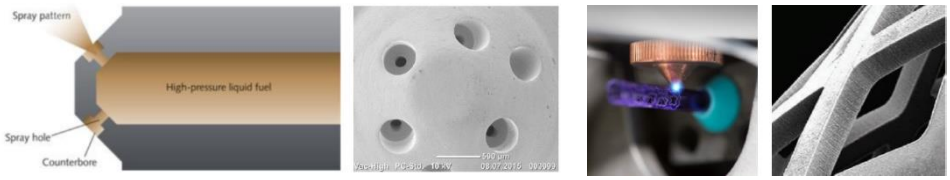

Figure 25. Femtosecond laser applications in micro-machining. Fuel injector nozzle drilling in steel or metal alloys (top), and medical stent manufacturing using nitinol tubes. Laser parameters for both processes: 40 W, 1 MHz, 300 fs, 1035 nm.

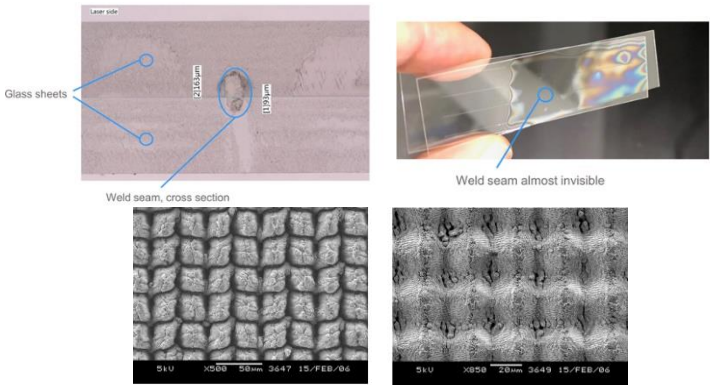

Figure 26. Emerging femtosecond laser micro-processing applications. Top: Glass Welding using 40 W, 1 MHz, 300 fs 1035 nm laser. A plasma is generated at the interface between the glass sheets (Left). Two-dimensional scanning allows generation of invisible weld seams (right). Glass-to-metal welding can also be realized. Bottom: micro-structuring of steel using a fs IR laser to generate a hydrophobic surface (to repel water). This application will require line beam focusing and average power levels up to several 100 W.

The main drivers for ultrafast laser processing are application in the micro-electronics manufacturing market, including flat panel display manufacturing and repair, wafer and panel cutting and advanced packaging (Fig.27-29). These processes work with lasers with 10 ps pulse duration, but sub-ps lasers are also being used. For both pulse duration regimes, the dominant laser wavelengths are in the ultraviolet range (343-355nm), followed by green (515 – 532 nm). The main reasons for using shorter wavelengths are the smaller spot sizes, which results in a smaller HAZ, and the increased linear absorption of the materials. Figure 27 shows OLED display foil cutting using 10 ps lasers at various wavelengths. By using ultraviolet laser light, the cut quality can be considerably improved compared to IR or green, with HAZ widths as low as 5 µm. The photo sequence at the bottom of Fig.27 shows how the decrease in pulse fluence, by increasing the repetition rate at the same power level of 30 W, leads to an increase of the cutting speed by almost a factor of 2, while considerably reducing the HAZ. This is a perfect demonstration of the importance of operating near the optimum pulse fluence. Other ultrafast laser applications in micro-electronics are wafer dicing, cutting of SIP and modified PI (Fig. 28), and percussion drilling in various materials (Fig. 29). Again, picosecond lasers emitting in the UV are dominant in these applications today.

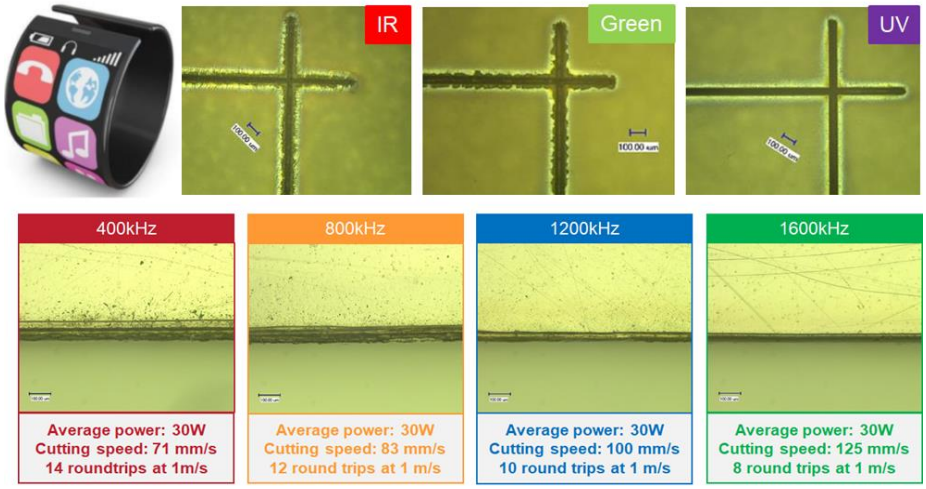

Figure 27. Polymer sandwich foil cutting in OLED display manufacturing. The linear absorption of the materials in the ultraviolet wavelength range leads to improved cut quality and smaller HAZ. Lasers used are UV lasers with 30 W average power, 10 ps or 500 fs pulse duration, 0.5 – 2 MHz repetition rate.

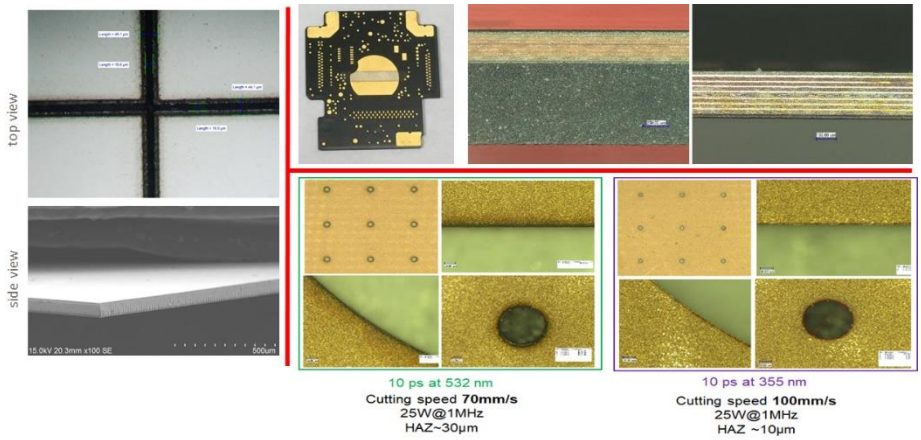

Figure 28. Ultrafast laser micro-processing applications in micro-electronics manufacturing. Silicon wafer dicing using fs green or ps UV lasers (left), cutting of SIP (system in package) using 50 W, 1 MHz, 10 ps, 532 nm laser (top right), cutting of modified Polyimide (Kapton), comparing 25 W, 1 MHz, 10 ps lasers at 532 nm and 355 nm (bottom right).

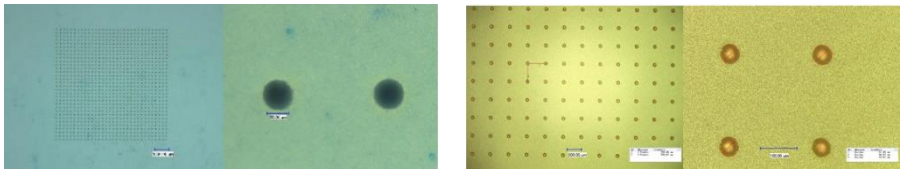

Figure 29. Ultrafast laser percussion drilling applications. Left: Drilling of 30 µm diameter holes in Low-Temperature Co-Fired Ceramics (LTCC) using a 50 W, 1 MHz, 10 ps laser at 532 nm with a drill rate of 2,500 holes per second. Right: High speed drilling of 50 µm diameter holes in Ajinomoto Build-up Film (ABF) on copper (30 µm thick) using a 10 W, 1 MHz, 10 ps laser at 355 nm with a drill rate of 3,000 holes per second.

A relatively large segment of the picosecond ultrafast laser machining market is the cutting of glasses, crystals and ceramics. These applications required infrared wavelengths and average power levels in the 100W range. Most cutting processes are ablative in nature as shown on the top part of Fig. 30. As was shown in Fig. 13, ablation rates at 1035 nm for glasses and ceramics can be as high as 1 mm^3/(W min), resulting in ablation rates in the range of 60 – 100 mm^3/min for a 100 W laser.

An alternative way of cutting glasses is filament-cutting, where the nonlinear Kerr-effect is used to generate a filament in the glass that can be many mm in length and a couple of microns in diameter. This usually requires operation in seeder burst mode with a pulse separation that is shorter than the typical plasma lifetime of 30 ns, or higher than 33 MHz seeder pulse repetition rate. Moving the focus laterally to generate a 'curtain' of filaments will lead to separation after parts of the substrate are heated with a continuous wave CO_2 or CO laser. Cutting speeds of greater than 1 m/s can be achieved for glass thicknesses of up to 5 mm with a surface roughness of less than 0.5 µm. In addition to glass and ceramic cutting, there are many other cutting, grooving, marking applications in various materials using infrared ps lasers.

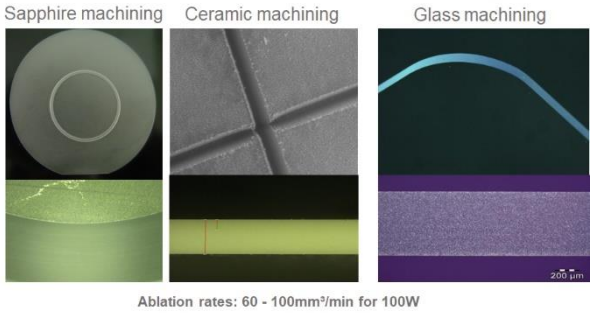

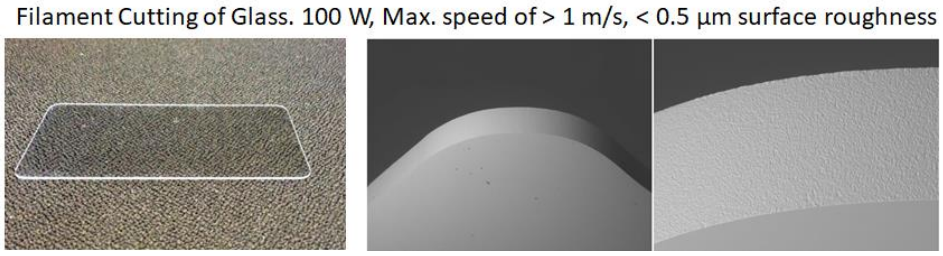

Figure 30. Cutting of glasses, sapphire and ceramics. Top: Ablative cutting of sapphire, ceramics and glass using a 100 W, 10 ps laser at 1064 nm. Typical ablation rates are in the range of 60 – 100 mm^3 per minute. Bottom: Filament cutting of glass using 100 W, 1064 nm, 10 ps lasers in seeder burst mode. A curtain of filaments with diameters of several microns is generated along the cut line. Separation is accomplished by irradiation with a low-power CO_2 laser (tens of W). The process speed is about 100 times faster as compared to ablative cutting.

7. SUMMARY AND CONCLUSION

Over the last decade, ultrafast lasers for micro-processing with pulse durations between 300 fs and 10 ps have penetrated the pulsed laser machining market at a CAGR of greater 10 % due to their ability to achieve relatively high ablation rates, as compared to nanosecond laser processing, with very small HAZ and high surface quality. To date, the world-wide market for these ultrafast lasers is estimated to be about 380 M$, with 60 % being served by picosecond lasers with output powers of up to 150 W in the infrared and pulse durations around 10 ps. The rest of the market is split 45/55 between femtosecond lasers for ophthalmic applications with output powers of less than 3 W in the infrared, and femtosecond lasers for non-ophthalmic micro-processing applications at power levels of up to 100 W in the infrared and 30 W in the ultraviolet. It is expected that the market for both ps and fs lasers, will continue to grow over the next five years at a CAGR of greater 10%, and possibly higher as new applications are being developed and implemented.
Independent of the laser wavelength, maximum ablation rates are achieved at average pulse fluences in the 0.5 – 2 J/cm^2 range for metals and semiconductors and between 4 and 6 J/cm^2 for transparent dielectrics. Measured maximum ablation rates are in the range of 0.1-0.3 mm^3/(W min) for metals and semiconductors, up to 0.8 mm^3/(W min) for glasses, and up to 8 mm^3/(W min) for transparent plastic materials. For metals, semiconductors and some plastics, highest ablation rates were consistently observed for sub-ps pulse durations. Ablation of materials that do not exhibit linear absorption at the laser wavelength, like transparent glasses and crystals, require longer pulse durations in the 10 - 20 ps range to maximize the ablation rate.

Shorter laser wavelength in the green and ultraviolet wavelength range will generally lead to decreased process speeds as compared to the infrared. However, the shorter wavelengths facilitate tighter focusing while maintaining the Rayleigh range of the beam, leading to finer cuts and a reduction in the HAZ. For this reason, pulsed UV lasers are dominant in applications in micro-electronic manufacturing, like OLED foil cutting, wafer dicing and hole drilling.

At any laser wavelength, operation at the optimum fluence not only maximizes the process speed but also leads to a reduction of the HAZ. In this case, the processing quality becomes independent of the pulse duration for pulses that are shorter than about 10 ps. To realize the low pulse fluences of about 1-2 J/cm^2, 100 W-class ultrafast lasers need to either be operated at repetition rates of around 10-20 MHz for the commonly used spot diameters of 20-30 µm, or the spot sizes are considerably increased, which would be an option for large area processing applications, like surface-texturing. If operation at high repetition rates is not feasible, seeder burst mode can be used to decrease the pulse energy to optimize the pulse fluence. However, ablation rates in seeder burst mode strongly depend on the number of pulses in the burst and the temporal gap between the pulses. If more than 5 pulses are used, and the temporal gap is much larger than the thermal relaxation time, the maximum ablation are similar to the ones that are observed for standard non-burst operation at the optimum pulse fluence.

Deployment of ultrafast lasers in pulsed laser applications will continue to grow and with the advent of new ultrafast laser processes and the need for increased throughput, the average infrared output power of both ps and fs laser in industrial applications will continue to be increased, moving from about 150 W to date to 300 W and potentially much more over the next five years. However, this will require operation at high repetition rates of greater 10 MHz and the development of faster scanning techniques. Small HAZ as the main advantage of ultrafast laser processing can only be realized if the heat per deposited per area and time remains low.

REFERENCES

[1] Strategies Unlimited, Lasers & Photonics Marketplace Seminar, PennWell 2016.

[2] C. Momma, B.N. Chichkov, S. Nolte, F. von Alvensleben, A. Tuennermann, H. Welling, B. Wellegehausen,"Short-pulse laser ablation of solid targets," Opt. Commun. 129, 134-142 (1996).

[3] S. Nolte, C. Momma, H. Jacobs, A. Tuennermann, B.N. Chichkov, B. Wellegehausen, H. Welling, "Ablation of metals by ultrashort laser pulses," J. Opt. Soc. Am. B14(10), 2716-2722 (1997).

[4] K.-H. Leitz, B. Redlingshoefer, Y. Reg, A. Otto, M. Schmidt, "Metal ablation with short and ultrashort laser pulses," Physics Procedia 12, 230-238 (2011).

[5] N. Hodgson, M. Laha, T. S. Lee, A. Steinkopff, and S. Heming,"Industrial Femtosecond Lasers and Material Processing," in: Industrial Laser Solutions, PennWell Publishing, January 22 (2019).
[6] S.I. Anisimov, B.L. Kapeliovich, T.L. Perel'man, "Electron emission from metal surfaces exposed to ultrashort laser pulses," Sov. Phys. JETP 39, 375-377 (1974).
[7] P.B. Corkum, F. Brunei, N.K. Sherman, T. Srinivasan-Rao, "Thermal response of metals to ultrashort-pulse laser excitation," Phys. Rev. Lett. 61, 2886-2889 (1988).
[8] N.K. Sherman, F. Brunei, P.B. Corkum, F.A. Hegman, "Transient response of metals to ultrashort pulse excitation," Opt. Eng. 28(10), 281114 (1989).
[9] T.Q. Qiu et al., "Short-pulse laser heating on metals," Int. J. Heat Mass Transfer 35(3), 719-726 (1992).
[10] J. Byskov-Nielsen, Short-Pulse Laser Ablation of Metals: Fundamentals and Applications for Micro-Mechanical Interlocking, PhD Thesis, Univ. of Aarhus, 2010.
[11] P. B. Johnson and R. W. Christy, "Optical constants of the noble metals," Phys. Rev. B 6, 4370 (1972).
[12] Z. Lin, L. V. Zhigilei, , University of Virginia, Department of Material Sciences,"Electron-Phonon coupling and Electron heat capacity in metals at high electron temperatures," collection of calculated data at: http://www.faculty.virginia.edu/CompMat/electron-phonon-coupling
[13] Z. Lin, L. V. Zhigilei, Temperature dependences of the electron-phonon coupling, electron heat capacity and thermal conductivity in Ni under femtosecond laser irradiation," Appl. Surface Science 253, 6295-6300 (2007).
[14] Z. Lin, L. V. Zhigilei, V. Celli, "Electron-phonon coupling and electron heat capacity of metal under conditions of strong electron-phonon nonequilibrium," Phys. Rev. B 77, 075133 (2009).
[15] D. Breitling, A. Ruf, F. Dausinger, "Fundamental aspects in machining of metals with short and ultrashort laser pulses," Proc. SPIE 5339, 49- 63 (2004).
[16] B. Jaeggi, B. Neuenschwander, M. Schmid, M. Muralt, J. Zuercher, U. Hunziker,"Influence of the Pulse Duration in the ps-regime on the ablation efficiency in metals," Physics Procedia 12, 164-171 (2011).
[17] B. Neuenschwander, B. Jaeggi, M. Schmid, V. Rouffiange, P.-E. Martin, "Optimization of the volume ablation rate for metals at different laser pulse-durations from ps to fs," Proc. SPIE 8243, 824307 (2012).
[18] B. Neuenschwander, B. Jaeggi, M. Schmid, "From ps to fs: dependence of the material removal rate and the surface quality on the pulse duration for metals, semiconductors and oxides," ICALEO 2012, 959-964 (2012).
[19] B. Neuenschwander, B. Jaeggi, M. Schmid, "From fs to sub-ns: dependence of the material removal rate on the pulse duration in metals," Physics Procedia 41, 794-801 (2013).
[20] N. Hodgson, S. Heming, A. Steinkopff, H. Haloui, and T.S. Lee, "Ultrafast laser ablation at 1035 nm, 517 nm, and 345 nm as a function of pulse duration and fluence", Lasers in Manufacturing (LIM 2019), paper Tu A_31-6 (2019).
[21] Y. Jee, M.F. Becker, R.M. Walser, "Laser induced damage on single crystal metal surfaces," JOSA B5, 648 (1988).
[22] G. Raciukaitis, M. Brikas, P. Gecys, B. Voisiat, M. Gedvilas, "Use of high repetition rate and high power ultrafast laser in microfabrication:How to keep the efficiency high," J. Laser Micro/Nanoengin. 4, 186-191 (2009).
[23] R. Knappe, H. Haloui, A. Seifert, and A. Nebel, Scaling ablation rates for picosecond lasers using burst micromachining" Proc. SPIE 7585, 7585-16 (2010).
[24] A. Zemaitis, M. Gaidys, M. Brikas, P. Gecys, G. Raciukaitis, M. Gedvilas, "Advanced laser scanning for highly-efficient laser ablation and ultrafast surface structuring: experiment and model," Nature, Scientific Reports, 8:17376, 1-14 (2018).
[25] B. Jaeggi, S. Remind, Y. Zhang, T. Kramer, and B. Neuenschwander, "Optimizing the specific removal rate with the burst mode under varying conditions," J. Laser Micro/Nanoengin. 12, 258-266 (2017).
[26] D.J. Foerster, S. Fass, S. Groeninger, F. Bauer, A. Michalowski, and E.R. Weber, T. Graf, "Shielding effects and re-deposition of material during processing of metals with bursts of ultrashort pulses," Appl. Surf. Sci. 440, 926-931 (2018).
[27] B. Bornschlegel and J. Finger, "In-situ Analysis of ultrashort pulsed laser ablation with pulse bursts," J. Laser Micro/Nanoengin. 14, 88-94 (2019).
[28] N. Hodgson, H. Allegre, A. Starodoumov, S. Bettencourt, "Femtosecond laser ablation in burst mode as a function of pulse fluence and intra-burst repetition rate," J. Laser Micro/Nanoengin. 15, 236-244 (2020).
[29] C. Kerse, H. Kalaycioglu, P. Elahi, B. Cetin, D. K. Kesim, Ö. Akcaalan, S. Yavas, M. D. Asik, B. Öktem, H. Hoogland, R. Holzwarth, and F. Ö. Ilday, "Ablation-cooled material removal with ultrafast bursts of pulses," Nature 537, 84-88 (2016).